Matter and Radiation at Extremes | RESEARCH ARTICLE | scitation.org/journal/mre

Overcritical electron acceleration and betatron radiation in the bubble-like structure formed by re-injected electrons in a tailored transverse plasma

Cite as: Matter Radiat. Extremes 8, 014403 (2023); doi: 10.1063/5.0121558
Submitted: 18 August 2022 • Accepted: 15 November 2022 •
Published Online: 7 December 2022

Yuan Zhao,[1,2,3] Haiyang Lu,[1,2,a)] Cangtao Zhou,[1,2,3,b)] and Jungao Zhu[1,2]

AFFILIATIONS

[1] Center for Advanced Material Diagnostic Technology and College of Engineering Physics, Shenzhen Technology University, Shenzhen 518118, People's Republic of China
[2] Shenzhen Key Laboratory of Ultraintense Laser and Advanced Material Technology, Shenzhen Technology University, Shenzhen 518118, People's Republic of China
[3] College of Optoelectronic Engineering, Shenzhen University, Shenzhen 518060, People's Republic of China

[a)] **Author to whom correspondence should be addressed:** luhaiyang@sztu.edu.cn
[b)] zcangtao@sztu.edu.cn

ABSTRACT

We present a novel scheme for dense electron acceleration driven by the laser irradiation of a near-critical-density plasma. The electron reflux effect in a transversely tailored plasma is particularly enhanced in the area of peak density. We observe a bubble-like distribution of re-injected electrons, which forms a strong quasistatic electromagnetic field that can accelerate electrons longitudinally while also preserving the electron transverse emittance. Simulation results demonstrate that over-dense electrons could be trapped in such an artificial bubble and accelerated to an energy of ~500 MeV. The obtained relativistic electron beam can reach a total charge of up to 0.26 nC and is well collimated with a small divergence of 17 mrad. Moreover, the wavelength of electron oscillation is noticeably reduced due to the shaking of the bubble structure in the laser field. As a result, the energy of the produced photons is substantially increased to the γ range. This new regime provides a path to generating high-charge electron beams and high-energy γ-ray sources.

I. INTRODUCTION

The laser-plasma accelerator (LPA) has shown extraordinary potential in the compact particle acceleration field since it was first put forward in 1979.[1–3] In the past few decades, a great deal of work on electron acceleration mechanisms has resulted in inspiring progress from the perspectives of theory, simulation, and experiment.[4,5] In principle, high-charge electrons can be accelerated in a laser field directly (direct laser acceleration, DLA) and by a laser wake field (laser wake-field acceleration, LWFA).[2] DLA, which occurs in an ion channel formed by the self-channeling effect, was first described by Pukhov *et al.*[6] It has been validated that this approach can produce an overcritical electron beam because it can be applied to near-critical-density (NCD) plasmas or even at the surface of solid-density plasmas.[7–9] However, it is challenging to maintain the electron beam quality owing to the tremendous impact of the laser field.[10] Unlike in DLA, electrons are accelerated longitudinally and confined transversely in LWFA. In addition, the accelerating gradient of the wake field is independent of the radial position, while the transverse confinement force increases with radius. These two features are capable of conserving electron beam qualities such as the energy spread, emittance, and divergence.[11] Meanwhile, the population of the witness bunch is restricted by the low fraction of electron self-trapping.[2,12] Various schemes have been proposed to resolve the population limitation of self-injection, including ionization injection in high-Z gas,[13,14] density

transitions,[15] irradiation of the wake field with another laser beam propagating in the vertical direction,[16] and bow-wave injection.[17] The electron charge is significantly enhanced from tens to hundreds of pC.[18] When increasing the power of the incident laser to hundreds of TW or even to the PW scale, the maximal charge can reach up to several nC.[19–21] Despite this, the LWFA total charge performance, particularly for high-energy electrons, is still not comparable to those of conventional radio-frequency sources.

The tailored plasma offers the possibility of improving beam quality through its remarkable contribution to LPA.[22–24] The mechanism behind the tailored plasma is the rapid changing of the wavelength of the plasma wave through introduction of a density transition, as the electron plasma frequency is proportional to the electron density, i.e., $\omega_{pe} \propto n_e$. Bulanov *et al.* first studied the excitation of a plasma wave in an inhomogeneous plasma in 1998.[25] In their regime, the phase velocity of the plasma decreased with a moderate decline of the plasma density in the laser propagating path. When the plasma phase velocity dropped to the quiver velocity of the background electrons, the Langmuir wave was broken. As a result, the electrons were trapped in the acceleration phase. The condition was totally different when the longitudinal density ramp was sharpened, i.e., $k_p L_s < 1$. Suk *et al.* showed that enormous numbers of electrons that were initially at the tail of a high-density wake field could enter the accelerating phase of the wake field as the plasma wavelength rose with a rapid density reduction.[26] Numerous efforts to optimize the gradient, scale length, and density profile have been invested to obtain high-charge electron beams in LWFA.[27–29] Unlike in a longitudinal density transition, a transverse density gradient is employed in LWFA to tilt the propagation axis of the laser pulse and induce wake-field asymmetry. As a result, it can considerably boost betatron oscillation and increase both the yield and energy of the produced photons.[30,31] In order to increase the amount of charge in an accelerated electron bunch, further design improvements of the plasma density profile are still required.

In this paper, we propose a new scheme that utilizes a bubble-like structure formed by electron reflux to accelerate a high-charge electron beam. This is achieved via tailoring the plasma density transversely, which results in a curvature of the plasma wavefronts and thus controls the electron re-injection along the maximal plasma density. The electrons inside the bubble shape feel a strong longitudinal field that acts as the acceleration field and a varying transverse field that confines the electron oscillation in the vertical direction. Simulation results show that an over-critical-density electron beam is injected into the bubble and efficiently gains an energy of 500 MeV. Furthermore, the frequency of betatron oscillation ω_β is adjusted by the laser beam to ten times that in LWFA. This significantly raises the cut-off energy of the emitted photons to the range of MeV.

II. ELECTRON REFLUX

In a uniform plasma medium, the group velocity of a relativistic laser beam $(a_0 \gg 1)$ is estimated to be $v_g(r)/c \approx 1 - \omega_p^2/\sqrt{2}\omega_0^2 a(r)]$.[32] In this expression, c is the speed of light in vacuum, ω_p and ω_0 denote the frequencies of the plasma wave and the laser, and $a(r)$ is the dimensionless laser intensity. Depending on the spatial profile of the incident laser beam, the plasma wavefronts in a uniform plasma show phase differences in the transverse direction. For example, the plasma wavefronts driven by a Gaussian laser beam look like a cone[33] [see the black line in Fig. 1(a)]. When introducing a transverse density gradient, ω_p in the group velocity formula is not constant, which helps further bend the plasma wavefront. Assuming a plasma with an initial density profile of the form $n_e(r) = n_{e0} \exp\{-(r - 1(\mu\text{m}))/(\sigma/2)\}$, where n_{e0} is the maximum electron density and σ denotes the waist radius of the laser beam, the red solid line in Fig. 1(a) shows the phase difference after traveling for a period of $20T_0$. Here, the situation is simplified to a 2D model,

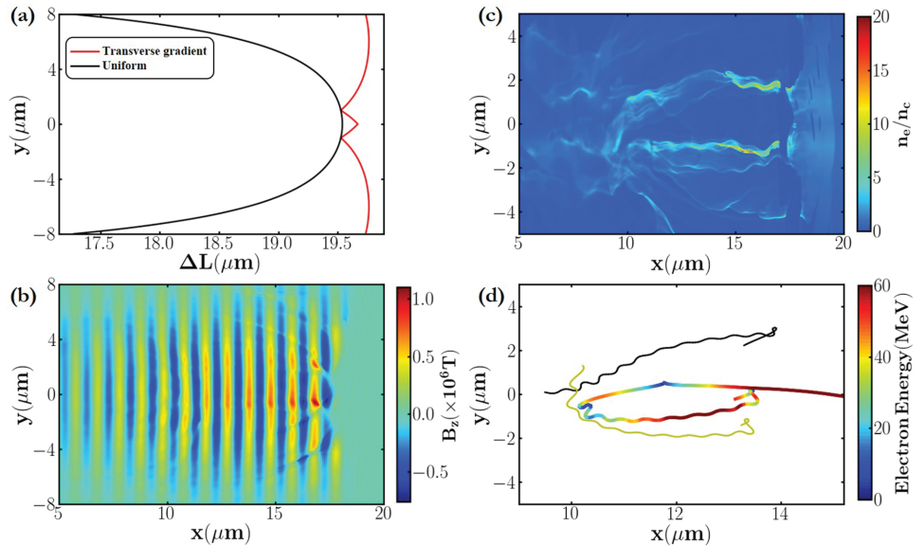

FIG. 1. (a) The phase differences of the plasma wave after $20T_0$ passage in a transversely tailored plasma (red solid line) and a uniform plasma (black solid line). The spatial distribution of the transverse magnetic field B_z (b) and the backward electron density (c) at $20T_0$. (d) A few typical trajectories of the re-injected electrons.

TABLE I. Simulation parameters.

(0.5 mm) parameters	Values
Lasers	
Laser intensity I_0	5×10^{21} W cm^{-2}
Laser wavelength λ_0	1 μm
Laser period T_0	3.33 fs
Waist radius of laser beam σ	6 μm
Full duration at half maximum $\sqrt{2 \ln 2}\tau_L$	39.2 fs
Target	
Material	Aluminum
Electron density n_{e0}	$2n_c$
Plasma length L_0	35 μm
Initial electron temperature T_e	10 eV

which omits the profile of the laser pulse and the plasma cell in the third dimension. The computational parameters of the laser and the plasma are given in Table I. It is worth pointing out that there are obvious phase delays of the plasma wave at places with the peak plasma density. The laser rays arriving at the curved wavefronts are efficiently refracted. The corresponding refractive index is written as $\eta(r) = \left\{1 - \omega_p^2(r)/\omega^2[1 + a^2(r)/2]^{1/2}\right\}^{1/2}$. It is apparently influenced by the laser profile following a function of $-\exp(r^2/\sigma^2)$ for a standard Gaussian laser beam, while the dependence on the electron density can be described as $-\exp[-(r - 1(\mu\text{m}))/(\sigma/2)]$. The resulting refractive index follows the gradient of the initial electron density. In other words, the laser rays are bent along the density transition.

We simulate the laser irradiating the transversely tailored plasma with the particle-in-cell (PIC) code EPOCH2D. To facilitate comparisons, the simulation parameters are kept the same as those used in the aforementioned theoretical calculation, as listed in Table I. The sampled window is $X \times Y = 40 \times 30$ μm^2 with cell numbers of $N_x \times N_y = 2000 \times 1500$. A Gaussian laser beam is incident from the left boundary of the simulation box. According to the expression for the group velocity in the previous paragraph, the impact of the laser wavelength is on the term ω, which is independent of the density profile. Therefore, the curvature at the plasma front can be observed under various laser wavelength conditions. The laser wavelength used in the simulations is 1 μm, corresponding to a critical plasma density of $n_c = 1.1 \times 10^{27}$ m^{-3}.[34] The plasma slab is located in the domain of $5 \le x \le 40$ μm. We employ the same plasma density profile discussed in the last paragraph. The characteristic term $n_{e0} = 2n_c$. It is worth noting that such a typical density distribution could be obtained by ablating a channel built of an array of nanotubes in an experiment.[35] In fact, such a density profile has already been fabricated with hydrogen gas in a laboratory with the hydrodynamical expansion of an optical-field-ionized plasma.[36]

Figure 1(b) shows the magnetic field at $20T_0$ and the visible curvature of the wavefront. The influence of the bent phase front has two aspects. On the one hand, it gives rise to the refraction of laser rays and shapes the laser profile into a particular distribution in the transverse direction. As displayed in Fig. 1(b), the light field is particularly weak in the region of the maximal electron density. On the other hand, the reflected laser field travels with a small angle with respect to the axis and then produces several off-axis peaks of the laser field. This causes the direction of the ponderomotive force to vary in the vertical direction. From Fig. 1(b), it is seen that there are zones close to the density peaks where the transverse ponderomotive force and the magnetic field share the same direction. For example, if they are both positive, the electrons in these areas will move up. Hence, the force $\boldsymbol{v} \times \boldsymbol{B}$ acts on the electrons in the negative x direction. Together with the space-charge force caused by the plasma charge separation, the electrons could be accelerated backward. However, it is relatively difficult to pull electrons back within the channel between the two density peaks. In view of the spatial distribution of the reflux electrons, the enhanced electron re-injection at the two maximal densities comprises a bubble-like structure with a maximum density on the bubble wall of over $20n_c$ [see Fig. 1(c)]. Figure 1(d) presents several representative trajectories of the backward electrons. As expected, the re-injected electrons finally flow into the tail of the laser pulse after experiencing continuous acceleration and deceleration processes owing to the intense ponderomotive force of the laser.

The self-generated electromagnetic field in the formed bubble resembles that in the laser wake field. It is beneficial to the electron acceleration in two ways. First, an acceleration phase for the electrons appears in the spatial distribution of the longitudinal field as a result of the charge separation [see Fig. 2(a)]. Second, the strong transverse field due to the over-dense electron reflux contributes to confining the witness electrons [see Fig. 2(b)]. It is worth mentioning that the re-injected electrons keep colliding with the laser field and oscillate in the transverse direction as they stream back with respect to the laser pulse. Hence, the bubble structure shakes with the propagation of the laser beam [see Fig. 2(d)]. In spite of this, the acceleration and focusing fields are ideal for electron acceleration.

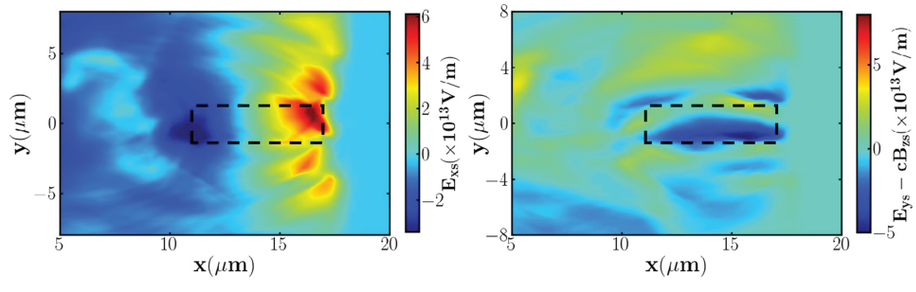

FIG. 2. The spatial distribution of the longitudinal electrostatic field (a) and the transverse field $E_{ys} - cB_{zs}$ in the (x, y) plane (b) at $20T_0$. The black dashed box marks the position of the bubble.

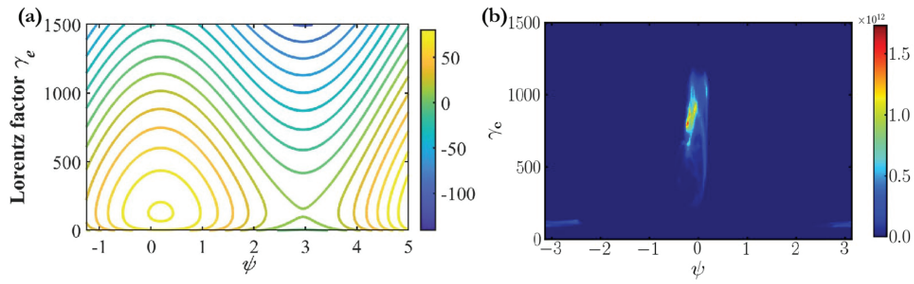

FIG. 3. (a) The Hamiltonian and (b) the electron density distribution in phase space (ψ, γ). The terms in (6) are normalized with the simulation results for the fields and the electron motion. It follows that $eE_L/m_e\omega_0 c = 50$, $eE_{Sx}/m_e\omega_0 c = 9.32$, $k_E = eE_{Sy}/m_e\omega_0^2 = 1$, $k_B = eB_{Sz}c/m_e\omega_0^2 = 1.47$, $v_y = 0.2$, and $v_x = 0.98$.

III. FORWARD ELECTRON ACCELERATION

In the rear of the bubble, a fraction of the re-injected electrons are trapped in the acceleration phase because the ponderomotive force of the laser pulse promotes them from fluid orbits into trapped orbits. The electron dynamics of self-trapping can be described as[37,38]

$$\frac{\mathrm{d}\gamma\, m_e v_y}{dt} = -e[(E_L + E_{Sy}) + v_x \times (B_L + B_{Sz})], \tag{1}$$

$$m_e c^2 \frac{\mathrm{d}\gamma}{\mathrm{d}t} = -e(v_y E_L \cos\psi + v_x E_{Sx}), \tag{2}$$

where γ, v_x, and v_y are the Lorentz factor, the longitudinal velocity, and the transverse velocity of the trapped electron, respectively, and m_e is the electron mass at rest. The electrons see both the laser field and the quasi-static self-generated field. E_L and B_L are the electric and magnetic fields of the driving laser. Similarly, E_{Sy}, E_{Sz}, and B_{Sz} are the components of the static electric field and the self-generated magnetic field in the plasma. The angle $\psi = \varphi - \phi$ represents the relative angle between the electron motion and the laser field. φ and ϕ denote the polar angles of the electron momentum and the laser electric vector, respectively. Since the electrons move in the laser propagation direction, the terms for the electric and magnetic fields from the laser in (1) are approximately counterbalanced.

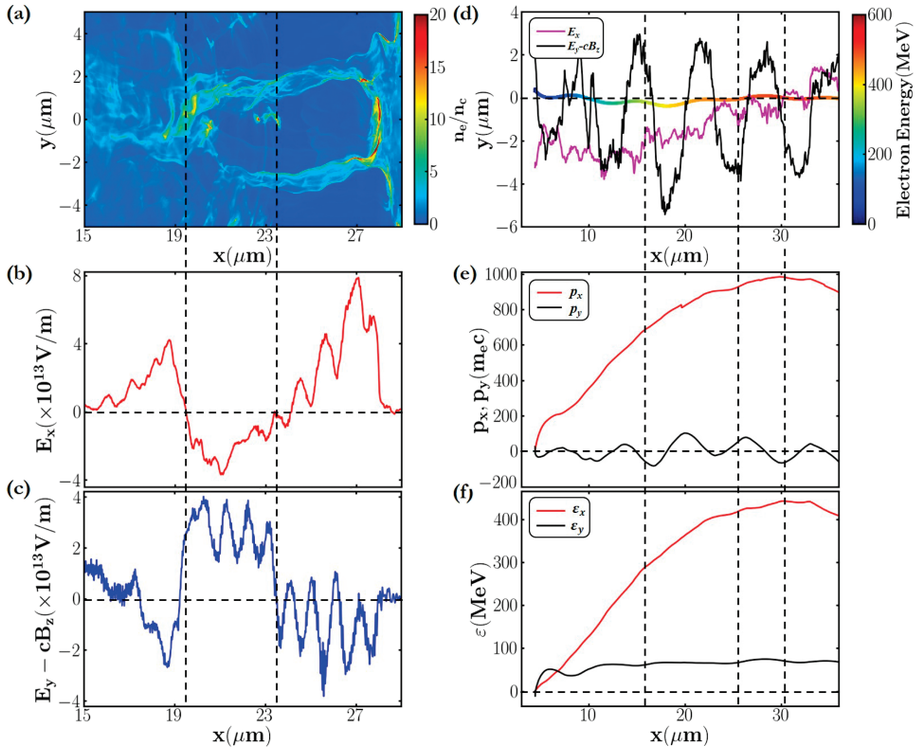

FIG. 4. (a) The spatial distribution of the plasma electron density at $32T_0$. (b) and (c) are plots of the on-axis longitudinal electric field E_x and the transverse field $E_y - cB_z$, respectively. (d) The trajectory of a sample electron and the electromagnetic field that the electron experiences. (e) The evolution of the transverse and longitudinal momenta, normalized by $m_e c$, for the same electron. (f) The work done by the longitudinal and transverse fields. The two vertical dashed black lines in (a)–(c) mark the acceleration zone. The first and second vertical dashed lines in (d)–(f) show the start of the betatron resonance acceleration, while the third dashed line marks the end of the wake-field acceleration. The horizontal dashed line in (b)–(f) gives the zero value of the corresponding quantity.

Under this circumstance, the electrons undergo transverse oscillation owing to the impact of the quasi-static fields. Following previous work, the self-generated fields can be simplified to be $E_{Sy} = k_E y$ and $B_{Sz} = -k_B y$, where k_E and k_B are constants.[6] The angular frequency of the electron motion is therefore expressed as

$$\frac{d\varphi}{dt} = \omega_\beta = \sqrt{\frac{e}{\gamma m_e}(v_x k_B + k_E)}. \tag{3}$$

The laser frequency witnessed by the trapped electrons is written as

$$\frac{d\phi}{dt} = (1 - v_x/v_{ph})\omega_0, \tag{4}$$

where v_{ph} is the phase velocity of the laser in the plasma. It follows that the time derivative of the relative phase between the electron momentum and the laser field is derived as[38]

$$\frac{d\psi}{dt} = \frac{d\varphi}{dt} - \frac{d\phi}{dt} = \sqrt{\frac{e}{\gamma m_e}(v_x k_B + k_E)} - (1 - v_x/v_{ph})\omega_0. \tag{5}$$

A Hamiltonian in phase space (ψ, γ) is then given by

$$H = \frac{e}{m_e c^2} v_y E_L \sin\psi + \frac{e}{m_e c^2} v_x E_{Sx}\psi + 2\sqrt{\frac{e}{m_e}(v_x k_B + k_E)\gamma} - (1 - v_x/v_{ph})\omega_0\gamma. \tag{6}$$

The separatrix and fixed point are solved by letting the right-hand side in (2) and (5) equal zero. That is, $\psi_c = \arccos(-v_x E_{Sx}/v_y E_L) + 2n\pi$ and $\gamma_c = e(v_x k_B + k_E)/m_e(1 - v_x/v_{ph})^2\omega_0^2$. Figure 3(a) shows the Hamiltonian in phase space (ψ, γ). It is apparent that electrons that initially reside around the fixed point feel slow phase movements and can stay in the acceleration phase for a long time. The electron density is plotted in the same phase space (ψ, γ) [see Fig. 3(b)], and is consistent with the above theoretical discussion.

Figure 4(a) shows that electrons with a maximum density of $\sim 22 n_c$ are self-injected into the bubble. The longitudinal and transverse fields on-axis are drawn in Figs. 4(b) and 4(c). The longitudinal electrostatic field has a maximum of $\sim 4 \times 10^{13}$ V/m, which enables an extremely high acceleration gradient of 4×10^4 GV/m. Since the laser depletion is non-negligible in an NCD plasma, the group velocity of the laser is lower than that given before. For the parameter set in the simulated case, the phase velocity of the plasma wave v_p is approximately equal to the group velocity of the laser v_g, which is calculated as $\sim 0.86c$. Applying the relation $(1 - v_p/c)L_d = L_s$, the dephasing length L_d of the electrons is then derived as 28 μm. Here, the length of the acceleration phase L_s is around 4 μm, as shown in Fig. 2. At this point, it is possible to accelerate electrons to several hundreds of MeV. We see that the strength of the fields oscillates along the x-axis. Beyond the reasons discussed in Sec. II, including the presence of the laser field and the shaking bubble wall, the existence of the electrons inside the bubble creates a substantial disturbance. The underlying sources of the noise electrons streaming into the bubble are twofold. First, a small fraction of re-injected electrons penetrating near the peak plasma density collapse into the bubble on experiencing a strong enough transverse field [see Fig. 1(d)]. In addition, there are electrons re-injected from the bubble head, although their density is not comparable to those of the two plasma density peaks [see Fig. 1(c)]. In spite of the oscillating fields, the electrons remain in the accelerating and focusing region. One typical trajectory of an injected electron [see Fig. 4(d)] indicates that the electrons remain in the longitudinal acceleration field for an acceleration distance of ~ 28 μm and gain energy reaching up to ~ 500 MeV. The acceleration process is described by the evolutions of the phase space x–p_x, x–p_y and the work done by forces characterized by two terms, $\varepsilon_\parallel = -\int 2 v_x E_x dt$ and $\varepsilon_\perp = -\int 2 v_y E_y dt$

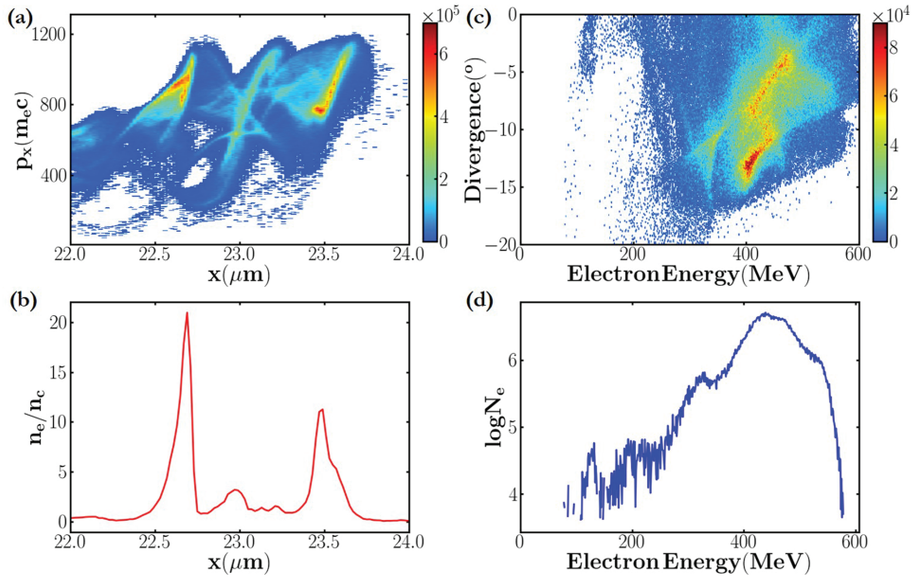

FIG. 5. (a) The phase space x–p_x of electrons inside the bubble at $32T_0$. (b) The longitudinal distribution of the electron density at the position with peak electron density. (c) The angular energy of the accelerated electrons. (d) The spectrum of the first electron microbunch.

[see Figs. 4(e) and 4(f)]. It is not surprising that the acceleration is mainly from the longitudinal electric field. In the transverse direction, the fields that the electrons meet, including the laser field and the self-generated electromagnetic field, shake strongly with the fluctuation of the electron bubble due to the existence of the laser pulse. Under this circumstance, the trapped electrons quiver in the bubble with a relatively short wavelength. This can be estimated by the distance that the electron travels before it slips by one laser wavelength, i.e., $\lambda_\beta = \lambda_0/(v_{ph}/v_x - 1) \approx 7\ \mu$m. As the oscillation frequency of an electron in the perpendicular direction is close to the laser frequency in the electron rest frame, the electron gains energy from the transverse field directly. However, this situation only occurs when the electron betatron oscillation matches the resonance condition $\omega_\beta \approx (1 - v_x/v_{ph})\omega_0$. Therefore, DLA mainly contributes in two cases. One is when the electron oscillation is dominated by the laser field, which happens at the beginning of the injection. The other comes with a high oscillation frequency caused by a strong transverse field [see Figs. 4(e) and 4(f)].

The phase space x–p_x of trapped electrons is shown in Fig. 5(a). It shows that the accelerated electrons are bunched at the laser frequency [see Fig. 5(a)]. This results from the oscillation of the self-generated electromagnetic field in the bubble because the bubble wall is quivering in the laser field. The density of the accelerated electron beams is overcritical [see Fig. 5(b)] and comparable with the electron density that could be obtained in DLA. The total charge of the electron bunches that are accelerated is as high as 0.26 nC. The angular energy distribution of the electrons, displayed in Fig. 5(c), shows great collimation in the high energy band. As expected, the spectrum of the electron bunch [sketched in Fig. 5(d)] is quasi-monoenergetic with a peak at ~440 MeV. It seems that these beam properties are much better than those achieved in DLA occurring in near-critical density plasmas. Overall, the electron beam obtained in the proposed scheme has the advantage of high density and great collimation and is an ideal combination of the DLA and LWFA acceleration regimes.

IV. BETATRON RADIATION

The transverse oscillation of high-charge electrons in a bubble-like structure could efficiently radiate a large number of photons in comparison with other radiation regimes involving bremsstrahlung and non-linear Compton scattering. As seen from Fig. 6(a), the peak density of a γ-ray is greater than $15n_c$. It is worth noting that the betatron oscillation period is extremely short because the quivering is affected by the laser field. Figure 6(b) shows that the transverse oscillation period is shorter than 20 μm, which is normally greater than 100 μm in LWFA.[39] As a result, it is possible to improve the energy of a radiated photon to the MeV level. Thanks to the high-quality electrons, the created photons are well collimated with a small divergence of ~10° [see Fig. 6(c)]. In principle, the energy of an emitted photon is related to the amplitude and frequency of electron oscillation. The critical frequency is expressed as $\omega_c = \frac{3}{2}K\gamma_e^2 2\pi c/\lambda_\beta$, where $K = \gamma_e\varphi$ is the dimensionless strength of the electron oscillation and is proportional to the Lorentz factor of the electron γ_e and the maximum tangential angle φ of the orbit. Applying the parameters of electron beam oscillation [see Figs. 5(d) and 6(b)], it is reasonable to attain a critical energy of 60 MeV in the photon spectrum [see Fig. 6(d)]. Taking the first photon pulse into consideration, the mean energy is calculated as 6.17 MeV. The number of photons at this average energy is 2.15×10^5 photons$(sr\ 0.1\%\ \mathrm{BW})^{-1}$. Hence, a striking brightness of 4.3×10^{22} photons s^{-1} mm^{-2} mrad^{-2} (0.1% BW)$^{-1}$ at an energy of 6.17 MeV is obtained. Such a bright MeV γ-ray source provides a new approach for compact light sources. In addition, thanks to the extremely short electron oscillation wavelength, the energy conversion efficiency from laser to γ-rays is improved to up to 0.2%, which

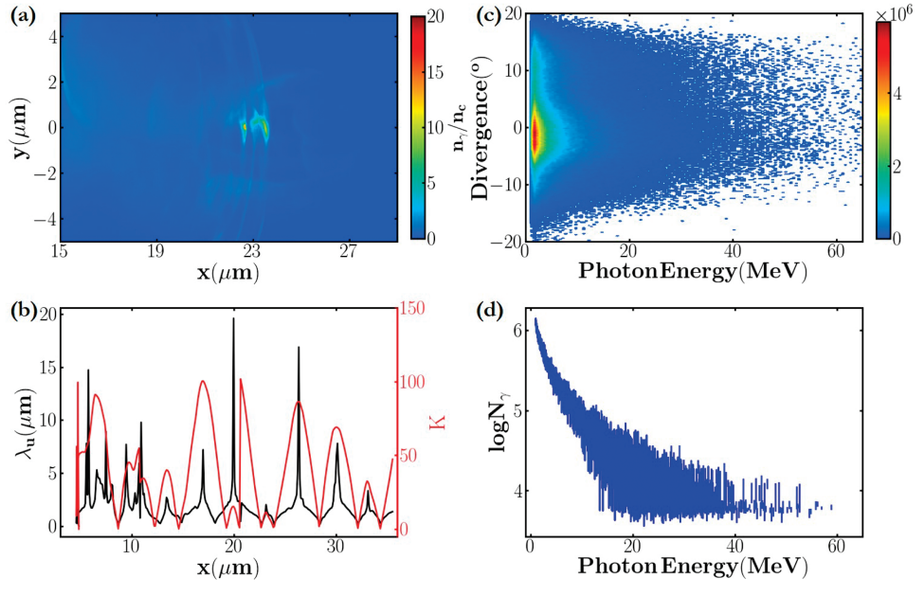

FIG. 6. (a) The emitted photon density at $32T_0$. (b) The evolutions of the local electron oscillation period (black solid line) and the local strength parameter K (*red solid line*). (c) The angle energy of the generated photons. (d) The spectrum of photons emitted by the first electron bunch.

further opens a path toward high-efficiency future laser-driven γ-ray sources.[40]

V. CONCLUSION

In conclusion, we have reported a new electron acceleration regime in a self-established bubble resulting from the special electron reflux in a laser interacting with a transversely tailored plasma. With a laser intensity of 5×10^{21} W/cm^2, simulations observe overcritical electron beams with a mean energy of 440 MeV and a total charge of up to 0.26 nC. Furthermore, the electron oscillation wavelength is extremely short — typically hundreds of μm in the classical betatron radiation occurring in a plasma wake field. A large number of photons in the γ-ray range are consequently radiated. This is a significant step in the investigation of betatron radiation. The described acceleration scheme is important to elucidate the physics underlying a laser irradiating a transversely inhomogeneous plasma. The generation of high-quality electrons and γ-rays should inspire the further development of LPA and compact radiation sources.

ACKNOWLEDGMENTS

This work was supported by the China Postdoctoral Science Foundation (Grant No. 2021M692204), the National Natural Science Foundation of China (Grant No. 11805278), the Fundamental Research Program of Shenzhen (Grant No. SZWD2021007), the Science and Technology on Plasma Physics Laboratory, the Guangdong Basic and Applied Basic Research Foundation (Grant No. 2022A1515010326), and the Shenzhen Technology University.

AUTHOR DECLARATIONS

Conflict of Interest

The authors have no conflicts to disclose.

Author Contributions

Yuan Zhao: Conceptualization (equal); Data curation (equal). **Haiyang Lu**: Supervision (equal). **Cangtao Zhou**: Writing – review & editing (equal). **Jungao Zhu**: Writing – review & editing (supporting).

DATA AVAILABILITY

The data that support the findings of this study are available from the corresponding author upon reasonable request.

REFERENCES

[1]T. Tajima and J. M. Dawson, "Laser electron accelerator," Phys. Rev. Lett. **43**, 267 (1979).
[2]E. Esarey, C. B. Schroeder, and W. P. Leemans, "Physics of laser-driven plasma-based electron accelerators," Rev. Mod. Phys **81**, 1229 (2009).
[3]S. M. Hooker, "Developments in laser-driven plasma accelerators," Nat. Photonics **7**, 775–782 (2013).
[4]A. J. Gonsalves, K. Nakamura, J. Daniels, C. Benedetti, C. Pieronek, T. C. H. de Raadt, S. Steinke, J. H. Bin, S. S. Bulanov, J. van Tilborg *et al.*, "Petawatt laser guiding and electron beam acceleration to 8 GeV in a laser-heated capillary discharge waveguide," Phys. Rev. Lett **122**, 084801 (2019).
[5]S. P. D. Mangles, B. R. Walton, M. Tzoufras, Z. Najmudin, R. J. Clarke, A. E. Dangor, R. G. Evans, S. Fritzler, A. Gopal, C. Hernandez-Gomez *et al.*, "Electron acceleration in cavitated channels formed by a petawatt laser in low-density plasma," Phys. Rev. Lett **94**, 245001 (2005).
[6]A. Pukhov, Z.-M. Sheng, and J. Meyer-ter-Vehn, "Particle acceleration in relativistic laser channels," Phys. Plasmas **6**, 2847–2854 (1999).
[7]C. Gahn, G. D. Tsakiris, A. Pukhov, J. Meyer-ter-Vehn, G. Pretzler, P. Thirolf, D. Habs, and K. J. Witte, "Multi-MeV electron beam generation by direct laser acceleration in high-density plasma channels," Phys. Rev. Lett. **83**, 4772 (1999).
[8]B. Liu, H. Y. Wang, J. Liu, L. B. Fu, Y. J. Xu, X. Q. Yan, and X. T. He, "Generating overcritical dense relativistic electron beams via self-matching resonance acceleration," Phys. Rev. Lett. **110**, 045002 (2013).
[9]Y. Tong-Pu, A. Pukhov, Z.-M. Sheng, F. Liu, and G. Shvets, "Bright betatronlike X rays from radiation pressure acceleration of a mass-limited foil target," Phys. Rev. Lett. **110**, 045001 (2013).
[10]T. W. Huang, C. T. Zhou, H. Zhang, S. Z. Wu, B. Qiao, X. T. He, and S. C. Ruan, "Relativistic laser hosing instability suppression and electron acceleration in a preformed plasma channel," Phys. Rev. E **95**, 043207 (2017).
[11]J. Krall, A. Ting, E. Esarey, and P. Sprangle, "Enhanced acceleration in a self-modulated-laser wake-field accelerator," Phys. Rev. E **48**, 2157 (1993).
[12]C. B. Schroeder, E. Esarey, B. A. Shadwick, and W. P. Leemans, "Trapping, dark current, and wave breaking in nonlinear plasma waves," Phys. Plasmas **13**, 033103 (2006).
[13]A. Pak, K. A. Marsh, S. F. Martins, W. Lu, W. B. Mori, and C. Joshi, "Injection and trapping of tunnel-ionized electrons into laser-produced wakes," Phys. Rev. Lett. **104**, 025003 (2010).
[14]M. Chen, Z.-M. Sheng, Y.-Y. Ma, and J. Zhang, "Electron injection and trapping in a laser wakefield by field ionization to high-charge states of gases," J. Appl. Phys. **99**, 056109 (2006).
[15]A. J. Gonsalves, K. Nakamura, C. Lin, D. Panasenko, S. Shiraishi, T. Sokollik, C. Benedetti, C. B. Schroeder, C. G. R. Geddes, J. Van Tilborg *et al.*, "Tunable laser plasma accelerator based on longitudinal density tailoring," Nat. Phys. **7**, 862–866 (2011).
[16]D. Umstadter, J. K. Kim, and E. Dodd, "Laser injection of ultrashort electron pulses into wakefield plasma waves," Phys. Rev. Lett. **76**, 2073 (1996).
[17]T. Z. Esirkepov, Y. Kato, and S. V. Bulanov, "Bow wave from ultraintense electromagnetic pulses in plasmas," Phys. Rev. Lett. **101**, 265001 (2008).
[18]J. Faure, C. Rechatin, O. Lundh, L. Ammoura, and V. Malka, "Injection and acceleration of quasimonoenergetic relativistic electron beams using density gradients at the edges of a plasma channel," Phys. Plasmas **17**, 083107 (2010).
[19]H. T. Kim, V. B. Pathak, K. Hong Pae, A. Lifschitz, F. Sylla, J. H. Shin, C. Hojbota, S. K. Lee, J. H. Sung, H. W. Lee *et al.*, "Stable multi-GeV electron accelerator driven by waveform-controlled PW laser pulses," Sci. Rep. **7**, 10203 (2017).
[20]G. Golovin, W. Yan, J. Luo, C. Fruhling, D. Haden, B. Zhao, C. Liu, M. Chen, S. Chen, P. Zhang *et al.*, "Electron trapping from interactions between laser-driven relativistic plasma waves," Phys. Rev. Lett. **121**, 104801 (2018).
[21]W. Lu, M. Tzoufras, C. Joshi, F. Tsung, W. Mori, J. Vieira, R. Fonseca, and L. Silva, "Generating multi-GeV electron bunches using single stage laser wakefield acceleration in a 3D nonlinear regime," Phys. Rev. Spec. Top.–Accel. Beams **10**, 061301 (2007).
[22]P. Tomassini, M. Galimberti, A. Giulietti, D. Giulietti, L. A. Gizzi, L. Labate, and F. Pegoraro, "Production of high-quality electron beams in numerical experiments of laser wakefield acceleration with longitudinal wave breaking," Phys. Rev. Spec. Top.–Accel. Beams **6**, 121301 (2003).
[23]A. V. Brantov, T. Z. Esirkepov, M. Kando, H. Kotaki, V. Y. Bychenkov, and S. V. Bulanov, "Controlled electron injection into the wake wave using plasma density inhomogeneity," Phys. Plasmas **15**, 073111 (2008).
[24]J. U. Kim, N. Hafz, and H. Suk, "Electron trapping and acceleration across a parabolic plasma density profile," Phys. Rev. E **69**, 026409 (2004).
[25]S. Bulanov, N. Naumova, F. Pegoraro, and J. Sakai, "Particle injection into the wave acceleration phase due to nonlinear wake wave breaking," Phys. Rev. E **58**, R5257 (1998).
[26]H. Suk, N. Barov, J. B. Rosenzweig, and E. Esarey, "Plasma electron trapping and acceleration in a plasma wake field using a density transition," Phys. Rev. Lett. **86**, 1011 (2001).

[27]L. T. Ke, K. Feng, W. T. Wang, Z. Y. Qin, C. H. Yu, Y. Wu, Y. Chen, R. Qi, Z. J. Zhang, Y. Xu *et al.*, "Near-GeV electron beams at a few per-mille level from a laser wakefield accelerator via density-tailored plasma," Phys. Rev. Lett. **126**, 214801 (2021).
[28]A. Buck, J. Wenz, J. Xu, K. Khrennikov, K. Schmid, M. Heigoldt, J. M. Mikhailova, M. Geissler, B. Shen, F. Krausz *et al.*, "Shock-front injector for high-quality laser-plasma acceleration," Phys. Rev. Lett. **110**, 185006 (2013).
[29]F. Y. Li, Z. M. Sheng, Y. Liu, J. Meyer-ter-Vehn, W. B. Mori, W. Lu, and J. Zhang, "Dense attosecond electron sheets from laser wakefields using an up-ramp density transition," Phys. Rev. Lett. **110**, 135002 (2013).
[30]M. Kozlova, I. Andriyash, J. Gautier, S. Sebban, S. Smartsev, N. Jourdain, U. Chaulagain, Y. Azamoum, A. Tafzi, J.-P. Goddet, K. Oubrerie, C. Thaury, A. Rousse, and K. Ta Phuoc, "Hard X rays from laser-wakefield accelerators in density tailored plasmas," Phys. Rev. X **10**, 011061 (2020).
[31]J. Ferri and X. Davoine, "Enhancement of betatron x rays through asymmetric laser wakefield generated in transverse density gradients," Phys. Rev. Accel. Beams **21**, 091302 (2018).
[32]P. Gibbon, *Short Pulse Laser Interactions with Matter: An Introduction* (World Scientific, 2005).
[33]M. Vranic, R. A. Fonseca, and L. O. Silva, "Extremely intense laser-based electron acceleration in a plasma channel," Plasma Phys. Controlled Fusion **60**, 034002 (2018).
[34]A. Macchi, *A Superintense Laser-Plasma Interaction Primer* (Springer, 2013)
[35]X. Zhang, T. Tajima, D. Farinella, Y. Shin, G. Mourou, J. Wheeler, P. Taborek, P. Chen, F. Dollar, and B. Shen, "Particle-in-cell simulation of x-ray wakefield acceleration and betatron radiation in nanotubes," Phys. Rev. Accel. Beams **19**, 101004 (2016).
[36]T. R. Clark and H. M. Milchberg, "Time and space-resolved density evolution of the plasma waveguide," Phys. Rev. Lett. **78**, 2373–2376 (1997).
[37]L. Ju, C. Zhou, K. Jiang, T. Huang, H. Zhang, T. Cai, J. Cao, B. Qiao, and S. Ruan, "Manipulating the topological structure of ultrarelativistic electron beams using Laguerre–Gaussian laser pulse," New J. Phys. **20**, 063004 (2018).
[38]R. Hu, B. Liu, H. Lu, M. Zhou, C. Lin, Z. Sheng, C.-e. Chen, X. He, and X. Yan, "Dense helical electron bunch generation in near-critical density plasmas with ultrarelativistic laser intensities," Sci. Rep. **5**, 15499 (2015).
[39]S. Corde, K. Ta Phuoc, G. Lambert, R. Fitour, V. Malka, A. Rousse, A. Beck, and E. Lefebvre, "Femtosecond x rays from laser-plasma accelerators," Rev. Mod. Phys. **85**, 1–48 (2013).
[40]S. Kneip, S. R. Nagel, C. Bellei, N. Bourgeois, A. E. Dangor, A. Gopal, R. Heathcote, S. P. D. Mangles, J. R. Marquès, A. Maksimchuk, P. M. Nilson, K. T. Phuoc, S. Reed, M. Tzoufras, F. S. Tsung, L. Willingale, W. B. Mori, A. Rousse, K. Krushelnick, and Z. Najmudin, "Observation of synchrotron radiation from electrons accelerated in a petawatt-laser-generated plasma cavity," Phys. Rev. Lett. **100**, 105006 (2008).